

Quantitative Detection in Lateral Flow Immunoassay Using Integrated Organic Optoelectronics

Vishak Venkatraman and Andrew J. Steckl¹, *Life Fellow, IEEE*

Abstract—A low cost, disposable point-of-care (POC) diagnostic device with integrated organic optoelectronic devices has been investigated for quantitative detection. The diagnostic component consists of a lateral flow immunoassay (LFIA) paper-based biosensor that uses capillary action for transportation of fluids. The absence of external fluid pumps and the low cost of materials utilized make LFIA a simple, inexpensive POC diagnostic device. For detection, the LFIA was integrated with organic optoelectronics devices on thin plastic sheets as a step toward a fully integrated lab-on-chip device. Organic semiconductor devices are suited for this purpose as they can be formed on many types of substrates and can have relatively large active area. For the light emitting component, phosphorescent green emitting organic light emitting diodes (OLED) have been used owing to their high brightness, while for the light detector an organic photodiode (OPD) that absorbs at green wavelengths has been used. Quantitative measurements were performed using optical transmission mode through the LFIA strip that forms red test and control lines by accumulation of gold nanoparticles (AuNP). In this configuration, the amount of transmitted light decreases as AuNPs accumulate on the test line, which directly correlates with the analyte concentration. This change in optical intensity results in a corresponding change in the measured OPD photocurrent. Initial quantification was obtained for 5 levels of rotavirus analyte. OLEDs and OPDs fabricated on plastic substrates were integrated within the LFIA chip to measure the intensity of line formation over a period of 30 min.

Index Terms—Lateral flow immunoassay, organic electronics, OLED, OPD, Au nanoparticles, immunochemistry.

I. INTRODUCTION

Point of care (PoC) test systems have multiple applications in the field of medical diagnostics [1]. Lab-on-chip (LoC) designs are integral components in such systems as they provide portability by miniaturizing laboratory scale equipment. The major goals of LoC systems are the integration and miniaturization of various functions and components, such as sample preparation, sensors and detectors, in order to reduce sample volume and measurement time [2].

Manuscript received September 10, 2017; accepted October 16, 2017. Date of publication October 18, 2017; date of current version November 22, 2017. This work was supported in part by the National Science Foundation (ENG 1236987) and in part by the industrial members of the Center for Advanced Design and Manufacturing of Integrated Microfluidics through NSF I/UCRC under Award IIP-1738617. The associate editor coordinating the review of this paper and approving it for publication was Prof. Sang-Seok Lee. (*Corresponding author: Andrew J. Steckl.*)

The authors are with the Electrical Engineering and Computer Science Department, University of Cincinnati, Cincinnati, OH 45221-0030 USA (e-mail: a.steckl@uc.edu).

Digital Object Identifier 10.1109/JSEN.2017.2764178

Paper-based microfluidic devices, such as lateral flow immunoassays (LFIA), have many such desirable characteristics: (a) capillary action for fluid transport in contrast to PDMS-based microfluidics, which require external pumps for operation; (b) use of paper-based components, such as nitrocellulose membranes, which are bio-sustainable [3]–[6] and roll-to-roll process compatible. The simplicity of construction and relatively low cost of materials results in low cost of manufacturing [7]. LFIAs work on the principle of immunoreaction, capturing antibodies tagged with gold nanoparticles (Au NP) in the test and control line regions of the membrane. Such capture leads to appearance of red colored lines, which are visually interpreted [8]. The presence of analyte in the fluid sample is indicated by the appearance of both test and control lines. The absence of analyte results in the appearance of the control line only. This type of analysis is useful for certain analytes, such as hcG hormones for pregnancy testing [9], where only a yes or no answer is needed. Other diagnostic tests require or prefer quantitative analysis [10]. Further, the visual interpretation of the lines in the LFIA can be somewhat subjective and/or altered by psychological misinterpretation. This problem can be reduced by incorporating fluorescence-based nanoparticles, which produce a much stronger visual signal [11]. We have previously reported the integration of organic light emitting diodes (OLED) as light sources to excite these fluorophores leading to increased sensitivity devices [12], [13]. However, these devices still do not provide quantitative information.

To offset some of these disadvantages, efforts have been undertaken [14] to integrate optical detection with the LFIA in order to make it a quantitative test, as well as to remove subjective perceptions. This type of design uses a light source in the form of a miniature LED and photodiode (PD) chips as light detectors [10]. When NPs accumulate at the test or control line, they absorb some of the incident light and thereby reducing the light intensity reaching the photodiodes and, hence, the photodiode current. The change in photocurrent is processed using analog microelectronic circuits, which typically drive an LCD unit to display a quantitative result. Such optical readers can be stand-alone units, into which the LFIA test strips with the formed test lines are inserted and read [15], [16]. External readers provide sophisticated functionality and can be extremely sensitive. However, they are generally too expensive for PoC use and are not fully portable [10]. A few integrated, packaged small devices are commercially available, but are

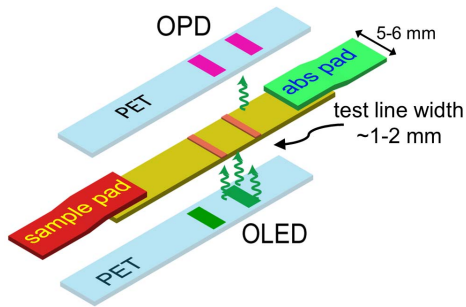


Fig. 1. Schematic diagram of integration approach of organic optoelectronics (light emission and detection) with LFIA (5-6 mm wide and 60-100 mm long).

predominantly semi-quantitative (2-3 levels) in nature [17]. They do alleviate the problem of subjective interpretation by providing the results in a digital display. The optical detection scheme in such systems use discrete component inorganic optoelectronics devices, such as surface mounted LEDs and PDs. Such an approach poses a major alignment challenge with the test line [10]. Furthermore, the detection is usually based on optical reflection, which requires that the LEDs and PDs be co-planar and, hence, wave guides are needed to direct light in order to minimize light intensity loss [10]. These requirements make the device bulky, less reproducible and prone to errors. Such devices can be fairly expensive and not environmentally friendly [18], as the entire plastic package with the on-board electronics is disposed after each use.

In this article, we describe the use of organic optoelectronics as light sources and detectors for integrating with the LFIA. OLEDs and organic photodiodes (OPDs) use thin films of organic materials to emit and detect light. The planar form factor of such devices has been utilized in plastic microfluidic system by Pais et al. to achieve significant improvement in limit of detection [19]. Organic devices can be formed at relatively low or room temperature and, hence, can be formed on plastic and other flexible substrates [20]. These substrates also facilitate integration in POC diagnostic systems and have been utilized by other groups [21]. In our group, we have previously reported [12] OLED fabricated on plastic integrated with LFIA. The next key step reported here is the OPD integration and quantitative analysis. An integration using optical transmission mode of analysis is illustrated in Fig. 1. OLEDs and OPDs can be fabricated on separate planar substrates, such as thin plastics, and integrated as layers directly with the LFIA membranes.

In this design, the optical alignment between light source, LFIA test line and photodetector is simpler and more accurate than in reflection mode designs. The ability to fabricate the organic electronics on thin plastic substrates facilitates increased light transmission through the LFIA membrane and detection by the OPD. The light source and detector are in close proximity in such a configuration and, hence, maximum signal generation and detection efficiency can be achieved, while the bulk of the overall package can be significantly reduced. The OLED and the OPD can be patterned to match the dimensions of the test lines, which is much

more desirable compared to the point source characteristics of the inorganic LEDs. The associated cost of such approach is significantly lower as the components can be roll-to-roll manufactured and integrated [22]. Finally, the devices can be fabricated with ecofriendly materials [23] and substrates making them environmentally friendly [24] and disposable [25].

In this project, we have used a commercial Au-NP based LFIA that forms lines that are normally red in color. In a properly functioning assay, two lines form in the presence of the biomolecule to be detected in the sample solution. The color intensity increases with the amount of analyte in the sample solution. Consequentially, the intensity of green light transmitted through the LFIA decreases as the analyte concentration increases [26]. In the next section, we describe the fabrication of these devices on glass and plastic substrates. Following the description of the fabrication process, device characteristics are discussed and compared. The devices on glass substrates exhibit superior performance compared to those on plastic substrates. To determine the best case quantitative analysis, devices fabricated on glass are integrated with LFIA with pre-formed test lines. However, ultimately devices fabricated on thin plastic substrates will be integrated within the LFIA package. The integration process is described and discussed in later sections. Instead of using analytes of different concentrations, we perform the equivalent process by measuring the intensity over time as additional analyte reaches the test line. This is because, for a given analyte concentration, the line requires a certain time period to fully form and saturate (~ 20 -30 min). During this period, the density of the test line gradually increases, which is then quantified in our experiments. Finally, in the Conclusions and Future Directions section, we describe how the signal can be analyzed using microelectronic components and illustrate a proposed prototype with promising results.

II. DEVICE FABRICATION AND CHARACTERIZATION

OLEDs were fabricated with a multi-layer structure containing a phosphorescence emission layer and other layers for enabling or blocking charge transport. This organic stack was selected due to its high efficiency and brightness, as demonstrated by the Forrest group [27]. In contrast, for OPDs, a simple single layer structure was chosen for simplicity based on a single light absorption layer [28].

Devices were fabricated on both glass and polymer (plastic) substrates. Device fabrication on glass (30mm \times 30mm) started by cleaning pre-patterned indium tin oxide (ITO) coated (900 μ m) substrates. The patterned ITO stripes were 2mm wide and had a sheet resistance of 10 Ω /square. This dimension fits well with the typical LFIA test line width (~ 1 -1.5 mm). Solvent cleaning in an ultrasonic bath was performed followed by mechanical scrubbing using clean wipes. Next, substrates were baked at 120 C to remove any residual solvents. The surface was then cleaned using O₂ plasma (250W power) exposure for 2 min. For devices on plastic (PET) substrates, ITO coated sheets (60 Ω /square) of 127 μ m thickness (Sigma Aldrich) were patterned using photolithography. More details of this fabrication process are found elsewhere [12]. The patterned ITO on plastic substrates,

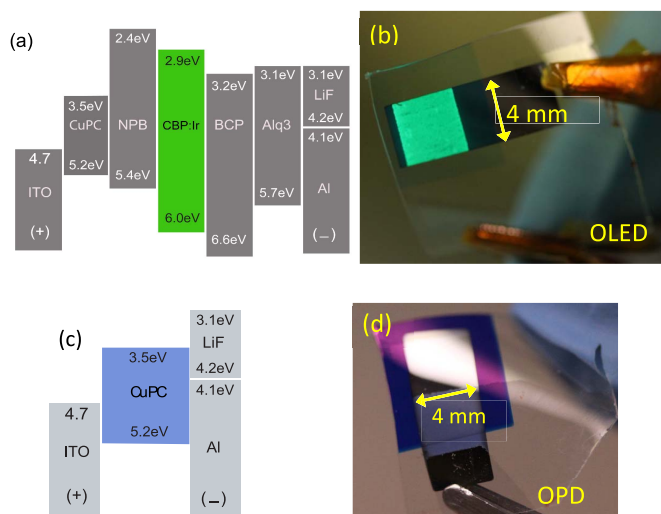


Fig. 2. Organic devices details: energy band diagrams for OLED (a) and OPD (c); photographs of OLED (b) and OPD (d).

had 4 mm wide stripes, for reasons explained later in the following sections.

The deposition procedure of the organic layers and metal cathode is the same for both glass and PET substrates. The layers were vacuum deposited sequentially in a high vacuum system (SVT Associates) at operating pressures of $\sim 5 \times 10^{-7}$ Torr. The stack and thickness of the layers were as follows: ITO[90 nm], CuPC[40nm], NPB[17 nm], CBP:Ir(ppy) 3(10 wt%)[30 nm], BCP[12 nm], Alq3[25 nm], LiF[<1 nm], Al[40 nm]. The thickness and deposition parameters were characterized using an in situ quartz crystal monitor. The organic layers were deposited through a shadow mask with a square opening to prevent deposition in unwanted areas, specifically the contact pads. For OLEDs, the combined organic layers had a total thickness of ~ 100 nm. For the OPD, a single thick layer of CuPC (500nm) was deposited using a similar shadow mask as for the OLED. The cathode (LiF/Al) was then deposited through a second shadow mask to create contact stripes with 4mm width. The devices fabricated on glass had an active area of 2mm \times 4 mm and 4 mm \times 4mm for the devices on PET substrates. The Al cathode (top electrode) is reflective and hence the emitted light exits the ITO electrode and substrate. The OLED bottom emitting configuration needs to be taken into consideration when integrating with the LFIA. For OPDs, the transmitted light also enters through the substrate and is absorbed in the CuPC layer, generating photocurrent in the device. Fig. 2 shows the devices fabricated on PET substrates and corresponding energy diagrams.

OLED devices were characterized under ambient room conditions for current – voltage (I-V) and brightness-voltage (L-V) characteristics. A luminance meter (Konica-Minolta CS-200) was used to measure the brightness while the applied voltage was swept at intervals of 0.25V from an Agilent DC power source controlled by LabVIEW software. The characteristics of devices on PET and glass are compared in Fig. 3 (a, b) (same dimensions of 2mm \times 4mm). They exhibited high brightness as can be expected from such devices [25]. The devices on PET did not perform quite as well as the devices on glass, primarily owing to the high resistance of ITO on

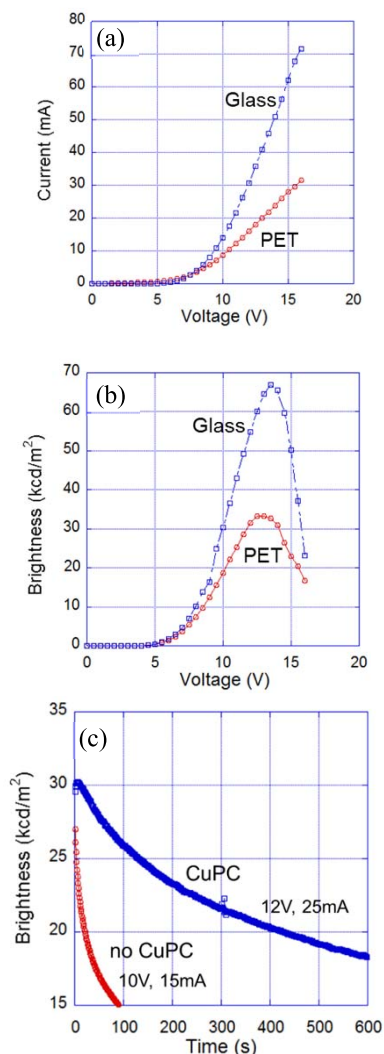


Fig. 3. OLED characteristics: (a) current vs. voltage; (b) brightness vs. voltage; and (c) lifetime testing on glass - brightness vs. time.

PET compared to that on glass. Hence, devices on glass were used to indicate possible best-case scenario results when integrating with the LFIA. However, devices fabricated on glass substrates are very thick (several mm) and rigid and cannot be integrated within the LFIA packaging. Lifetime performance is an important parameter for this particular application to produce reproducible results. Organic devices, particularly OLEDs, are susceptible to environmental moisture conditions. To improve the OLED lifetime performance, we incorporated a CuPC (40nm) capping layer, which has been reported [29] to be beneficial for this purpose. Lifetime of OLEDs fabricated on glass, with and without the CuPC layer, is shown in Fig. 3(c). However, this is outweighed by the significant improvement in lifetime.

For OPD characterization, I-V characteristics were measured with an HP picoammeter (model #4140B) using voltage steps of 0.1V. The absorption spectra of the active layer (deposited on quartz substrates) were measured using a Perkin Elmer spectrometer, see Fig. 4(a). The layer absorbs significantly in the green region, which can be expected from the purple color appearance of the layer. The I-V characteristics of OPD with CuPC layers of 250 and 500 nm are shown

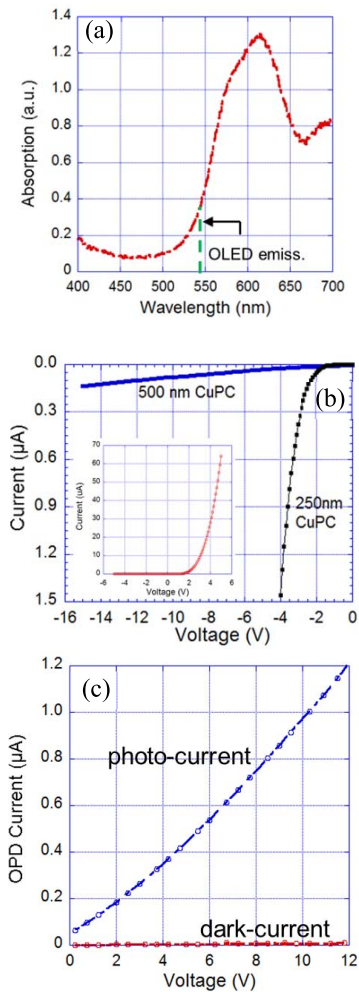


Fig. 4. OPD characteristics: (a) absorption spectrum of the active layer; (b) reverse bias dark current characteristics for 250 and 500 nm CuPC layers; and (c) photocurrent response of OPD in reverse bias, excited with a green laser source.

in Fig. 4(b). Not unexpectedly, the OPD with the thicker 500nm layer had a much reduced dark current and higher breakdown voltage and was, therefore, selected as the device thickness. The OPD responsivity was measured using a green laser (543nm, 1mW). A typical responsivity of 1.2 mA/W was obtained [Fig. 4(c)]. The OPT performance was found to be similar for both glass and PET substrates.

III. LFIA DIAGNOSTICS

Rotavirus test kits manufactured by Meridian Bioscience Inc. (Cincinnati, OH) were used in the LFIA experiments. The rotavirus antigen is detected using a sandwich immunoreaction at a specific location in the strip (test line) which contains antibodies (Ab) impregnated in the nitrocellulose membrane. The Abs bind to an epitope of the rotavirus protein. The conjugate pad of the assay strip contains gold nanoparticles (Au NPs) conjugated to Abs that attach to a different epitope of the virus protein. The sample solution is transported by capillary wicking through the assay kit. In the presence of the virus an Ab sandwich with the antigen is formed, which leads to the accumulation of the Au NPs in the narrow region of the test line. This results in a dark red line, whose

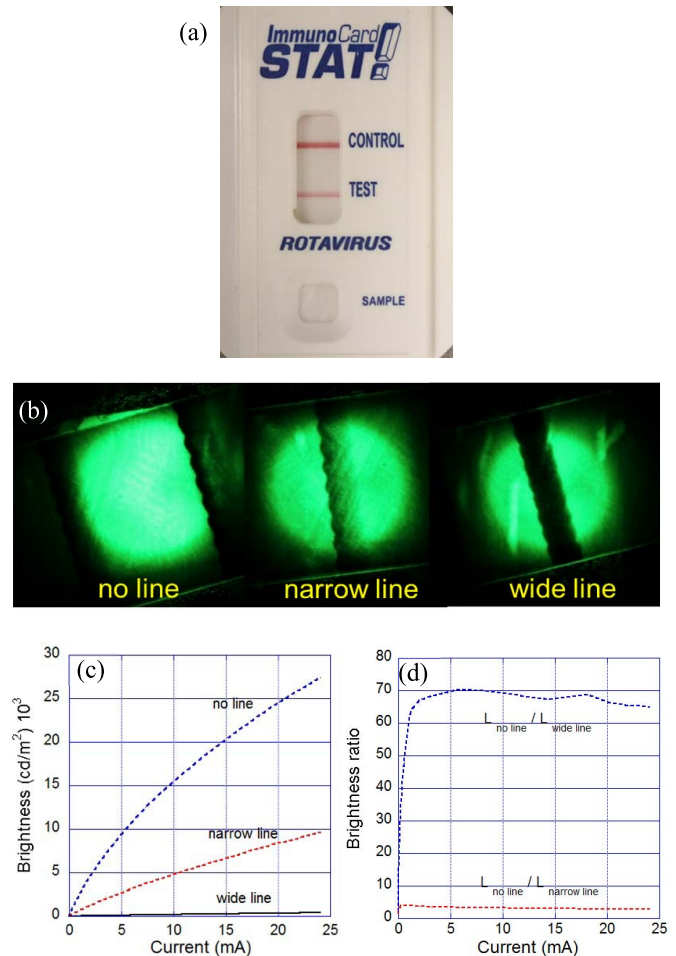


Fig. 5. LFIA details: (a) test and control lines formation; (b) optical density of test line under green LED illumination; (c) brightness of light transmitted through LFIA lines of different densities vs. green LED bias current; and (d) brightness ratio of no line/wide line and to no line/narrow line vs. green LED bias current.

intensity is roughly proportional to the amount of conjugated Abs captured, which in turn depends on the concentration of the rotavirus protein in the sample solution. To validate a successful test, these devices include a second stripe (the “control” line), which contains immobilized secondary Abs that can bind to the flowing conjugated Abs. This process occurs even in the absence of the analyte. Absence of this line invalidates the assay results (irrespective of formation of test lines). Ultimately, it is important to simultaneously detect both lines with optoelectronic circuits. However, in this manuscript a single line is detected at a time. This is done in order to reduce complexity for a proof-of-concept device, with visual verification of the performance of LFIA as intended. An example of a positive test result with the rotavirus assay is shown in the photograph of Fig. 5(a), where both the control and test lines are clearly visible.

The optoelectronic detection of these lines uses scattering of light by the accumulated Au NPs. Light transmission through the assay membrane is used to enable vertical integration of the LFIA strip with optoelectronic components, as illustrated in Fig. 1. The amount of light scattering increases with the number of captured Au NPs, which is directly related to an

increasing analyte concentration. This, in turn, reduces the transmitted light intensity. To validate this approach, a commercial LED package was utilized to illuminate test lines with various analyte concentrations. The photographs of Fig. 5(b), show images of the LFIA test lines under green light illumination. Increasing analyte concentration decreases the amount of green light passing through the test line, resulting in darker lines. This effect was confirmed by measuring the transmitted light intensity (brightness) as a function of LED current, as shown in Fig. 5(c). The brightness ratio between the “no line” to “wide line” and to “narrow line” cases was fairly constant with LED current (Fig. 5(d)), indicating a useful tolerance of variation in bias conditions and brightness.

IV. INTEGRATION

The initial integration of the organic optoelectronics and LFIA used OLEDs and OPDs fabricated on glass substrates due to their superior performance. The device dimensions used were $2 \times 4 \text{ mm}^2$. Assays were first run in original LFIA cassettes with various rotavirus concentrations in the analyte solution so as to obtain lines of varying density. The assays were run for 30 min. Then the active membranes with the test lines formed with various analyte concentrations were removed from the cassette and sandwiched between devices fabricated on glass. Alignment of the test line to the OLED and OPD was performed under an optical microscope. Alignment errors are compensated by having the device width (2 mm) larger than the typical test line width (1.2-1.5 mm). The OLEDs were typically biased to produce high brightness levels ($\sim 20\text{-}25 \text{ kcd/m}^2$) in order to obtain maximum sensitivity (as seen in Fig. 5).

The OPD current measured as the OLED voltage was swept from 0 to 15V is shown in Fig. 6(a) for different analyte concentrations (from zero to 100%) in the LFIA. For these measurements, the devices were biased beyond the point of peak emission intensity in order to determine maximum sensitivity. The OPD photocurrent monotonically decreases as the analyte concentration increases owing to less transmitted light passing through the sample. The maximum difference between the concentrations (i.e. the sensitivity) occurs at the maximum brightness peak, with a $\sim 200 \text{ nA}$ difference between the no analyte case and 100 % analyte. Current differences of this level can generally be detected with several types of microelectronic sensing circuits. The area under the curve (integrated OPD current) for each case is plotted against the analyte concentration in Fig. 6(b). A linear trend is observed between integrated OPD signal and analyte concentration, with fairly good reproducibility for repeated iterations ($n \geq 3$).

Following the performance analysis experiments with OLEDs fabricated on glass, the integration into the LFIA packaging was investigated using devices fabricated on thin plastic substrates that can be sandwiched within the cassette. The process starts with disassembling the various components of the LFIA stack (sample pad, NC membrane and conjugating pad) from the backing card. The position of the to-be-formed test lines are marked on the outer plastic packaging, for subsequent alignment of the OLED and OPD. The next step is attaching the OLED (device side) onto an

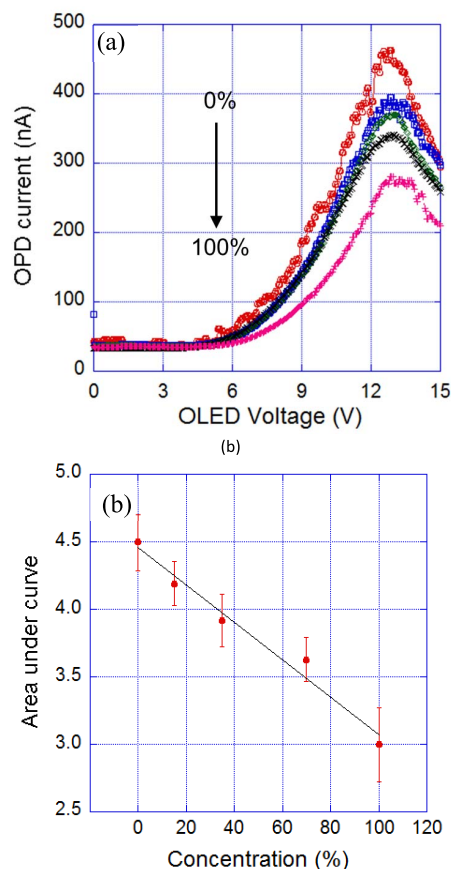


Fig. 6. Integrated OLED (glass)/LFIA/OPD measurements: (a) OPD photocurrent vs. OLED bias voltage for several analyte concentrations and (b) integrated photocurrent level (area under curve) vs. analyte concentration.

adhesive backing. The PET substrate measured $15 \times 15 \text{ mm}^2$. Copper tapes were attached to the OLED in order to make contact after the integration process. The NC membrane was then placed on top the PET substrate containing the OLED, with the control line aligning to the middle of the device area. The sample and the conjugate pads were then attached to the ends of the NC membrane. Finally, the PET substrate containing the OPD (same dimensions as the OLED) was attached to the top of the NC membrane. The top plastic casing of the LFIA cassette was attached to impart pressure on the sample pad and to contain the sample dispensing volume. The integration steps and photographs of the initial LFIA and final integrated OLED/LFIA/OPD package are shown in Fig. 7.

The integrated device was tested in a dark ambient optical room. A probe station equipped with a microscope was used to measure the photocurrent and dark currents of the OPD under OLED illumination. The OLED was powered using a LabVIEW controlled DC power source. The test was initiated by adding a “negative control” sample solution ($150 \mu\text{L}$) which leads to the formation of only the control line. The OLED was pulsed every 0.1 seconds and the corresponding OPD photocurrent was measured. Both the OLED and OPD devices were biased at a voltage of 10 V. As the line formed over time the OPD photocurrent decreased due to decreased light transmission as is evident in Fig. 8(a). To establish a baseline, the photocurrent was also measured in a region away from

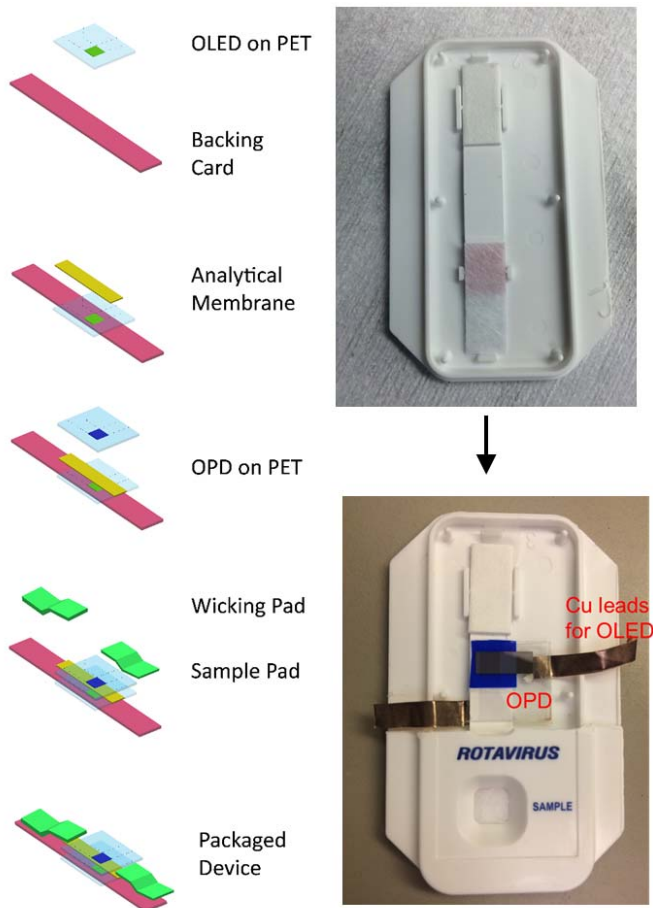


Fig. 7. Integration of organic optoelectronic devices (OLED and OPD) with LFIA strip inside the cassette.

the test line. In this case, there should be no decrease in light intensity transmitted, and, hence, photocurrent. Some minor decrease was observed, attributed to either “drying” effects of the LFIA (and hence transparency of the membrane) and/or organic device performance degradation over time. The *relative intensity* of the OPD current vs. time was obtained by subtracting the “no test” line signal from the overall test line signal, as shown in Fig. 8(b). To correlate the photocurrent data to the visual formation of the line, gray scale contrast of the line formation was obtained from the analysis of photographs taken over the same period of time. As can be seen in Fig. 8(c), the gray scale signal correlates well with the measured OPD current (Fig. 8(b)). One minor difference is that the OPD current seems to saturate more strongly than the visual signal after ~ 1000 s. This could also be attributed to variation in drying effects and/or the device performance degradation over time.

In addition to the integration of the optical source and detector, there are other necessary components (such as microelectronic circuits, power sources etc.) which are currently external and should be investigated for integration in the future. With fabrication techniques, such as hybrid assembly and the ever-decreasing size of IC chips [30], these components can also be fabricated or mounted on plastic substrates. For the power source, we have previously integrated a hybrid-manufactured NFC antenna circuit that harvests

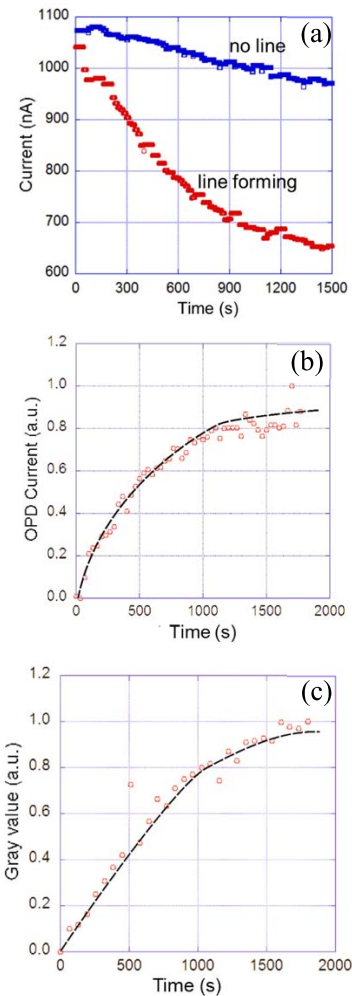


Fig. 8. Operation of integrated OLED/LFIA/OPD: (a) OPD photocurrent as LFIA test line over time; (b) relative OPD photocurrent (test line minus no line values) vs. time; and (c) gray scale values (from photographic images) as line forms over time (visual contrast).

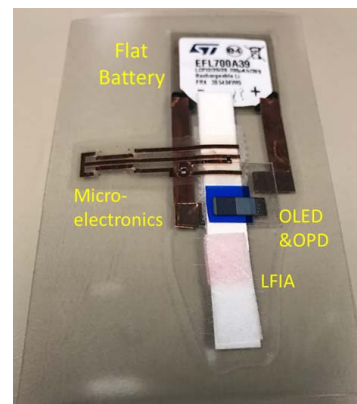


Fig. 9. Concept for fully integrated opto/microelectronics LFIA package. The OLED and OPD are on separate substrates, but have the same dimensions and are carefully superimposed.

RF power from smartphones [13]. Flat/flexible batteries are also an important option for providing electrical power in a package form factor that can be readily integrated [31].

In Fig. 9 such a proposed concept is shown, with the microelectronics that can be hybrid manufactured and the flat battery integrated along with the organic optoelectronic devices. While the prototype is not currently fully func-

tional, it is expected to be operational in the not too distant future.

V. CONCLUSION

In summary, a prototype of organic optoelectronics integrated with LFIA for multi-level (quantitative) detection has been demonstrated. This was accomplished by fabricating the OLED and OPD devices on thin plastic substrates, which were subsequently integrated within the LFIA package. The integration was designed to enable operation in optical transmission mode, such that the intensity of transmitted light decreases with increasing analyte concentration, resulting in decreasing OPD photocurrent.

ACKNOWLEDGMENT

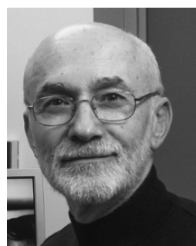
The authors gladly acknowledge the materials (LFIA test strip) generously provided by Meridian Bioscience Inc. and many helpful discussions with Ken Kozak.

REFERENCES

- [1] A. J. Tüdös, G. A. Besselink, and R. B. Schasfoort, "Trends in miniaturized total analysis systems for point-of-care testing in clinical chemistry," *Lab Chip*, vol. 1, no. 2, pp. 83–95, 2001.
- [2] P. Abgrall and A.-M. Gué, "Lab-on-chip technologies: Making a microfluidic network and coupling it into a complete microsystem—A review," *J. Micromech. Microeng.*, vol. 17, no. 5, p. R15, 2007.
- [3] E. Fu, S. A. Ramsey, P. Kauffman, B. Lutz, and P. Yager, "Transport in two-dimensional paper networks," *Microfluidics Nanofluidics*, vol. 10, no. 1, pp. 29–35, 2011.
- [4] A. W. Martinez, S. T. Phillips, G. M. Whitesides, and E. Carrilho, "Diagnostics for the developing world: Microfluidic paper-based analytical devices," *Anal. Chem.*, vol. 82, no. 1, pp. 3–10, 2009.
- [5] C. Parolo and A. Merkoçi, "Paper-based nanobiosensors for diagnostics," *Chem. Soc. Rev.*, vol. 42, no. 2, pp. 450–457, 2013.
- [6] A. K. Yetisen, M. S. Akram, and C. R. Lowe, "Paper-based microfluidic point-of-care diagnostic devices," *Lab Chip*, vol. 13, no. 12, pp. 2210–2251, 2013.
- [7] T. C. Tisone and B. O'Farrell, "Manufacturing the next generation of highly sensitive and reproducible lateral flow immunoassay," in *Lateral Flow Immunoassay*. New York, NY, USA: Humana Press (Springer), 2009, pp. 1–19.
- [8] P. Chun, "Colloidal gold and other labels for lateral flow immunoassays," in *Lateral Flow Immunoassay*. New York, NY, USA: Humana Press (Springer), 2009, pp. 75–93.
- [9] R. Tanaka *et al.*, "A novel enhancement assay for immunochromatographic test strips using gold nanoparticles," *Anal. Bioanal. Chem.*, vol. 385, no. 8, pp. 1414–1420, 2006.
- [10] K. Faulstich, R. Gruler, M. Eberhard, D. Lentzsch, and K. Haberstroh, "Handheld and portable reader devices for lateral flow immunoassays," in *Lateral Flow Immunoassay*. New York, NY, USA: Humana Press (Springer), 2009, pp. 157–184.
- [11] P. L. Corstjens *et al.*, "Up-converting phosphor technology-based lateral flow assay for detection of Schistosoma circulating anodic antigen in serum," *J. Clin. Microbiol.*, vol. 46, no. 1, pp. 171–176, 2008.
- [12] V. Venkatraman and A. J. Steckl, "Integrated OLED as excitation light source in fluorescent lateral flow immunoassays," *Biosensors Bioelectron.*, vol. 74, pp. 150–155, Dec. 2015.
- [13] V. Venkatraman, R. Liedert, K. Kozak, and A. J. Steckl, "Integrated NFC power source for zero on-board power in fluorescent paper-based lateral flow immunoassays," *Flexible Printed Electron.*, vol. 1, no. 4, p. 044001, 2016.
- [14] S. Kim and J.-K. Park, "Development of a test strip reader for a lateral flow membrane-based immunochromatographic assay," *Biotechnol. Bioprocess Eng.*, vol. 9, no. 2, pp. 127–131, 2004.
- [15] (2017). *BD Veritor System*. [Online]. Available: <https://www.bd.com/en-us/offers/capabilities/microbiology-solutions/point-of-care-testing>
- [16] (2017). *ESEQuant Lateral Flow Reader*. [Online]. Available: <https://www.qiagen.com/us/products/oem-services/ese-instruments/esequant-lateral-flow-reader/>
- [17] C. Gnoth and S. Johnson, "Strips of hope: Accuracy of home pregnancy tests and new developments," *Geburtshilfe Frauenheilkunde*, vol. 74, no. 7, pp. 661–669, 2014.
- [18] R. Widmer, H. Oswald-Krapf, D. Sinha-Khetriwal, M. Schnellmann, and H. Böni, "Global perspectives on e-waste," *Environ. Impact Assessment Rev.*, vol. 25, no. 5, pp. 436–458, 2005.
- [19] A. Pais, A. Banerjee, D. Klotzkin, and I. Papautsky, "High-sensitivity, disposable lab-on-a-chip with thin-film organic electronics for fluorescence detection," *Lab Chip*, vol. 8, no. 5, pp. 794–800, 2008.
- [20] A. Sugimoto, H. Ochi, S. Fujimura, A. Yoshida, T. Miyadera, and M. Tsuchida, "Flexible OLED displays using plastic substrates," *IEEE J. Sel. Topics Quantum Electron.*, vol. 10, no. 1, pp. 107–114, Jan. 2004.
- [21] G. Williams, C. Backhouse, and H. Aziz, "Integration of organic light emitting diodes and organic photodetectors for lab-on-a-chip bio-detection systems," *Electronics*, vol. 3, no. 1, pp. 43–75, 2014.
- [22] S. R. Forrest, "The path to ubiquitous and low-cost organic electronic appliances on plastic," *Nature*, vol. 428, no. 6986, pp. 911–918, 2004.
- [23] A. J. Steckl, "Circuits on cellulose," *IEEE Spectr.*, vol. 50, no. 2, pp. 48–61, Feb. 2013.
- [24] E. F. Gomez, V. Venkatraman, J. G. Grote, and A. J. Steckl, "Exploring the potential of nucleic acid bases in organic light emitting diodes," *Adv. Mater.*, vol. 27, no. 46, pp. 7552–7562, 2015.
- [25] S. Purandare, E. F. Gomez, and A. J. Steckl, "High brightness phosphorescent organic light emitting diodes on transparent and flexible cellulose films," *Nanotechnology*, vol. 25, no. 9, p. 094012, 2014.
- [26] A. K. Ellerbee *et al.*, "Quantifying colorimetric assays in paper-based microfluidic devices by measuring the transmission of light through paper," *Anal. Chem.*, vol. 81, no. 20, pp. 8447–8452, 2009.
- [27] C. Adachi, M. A. Baldo, M. E. Thompson, and S. R. Forrest, "Nearly 100% internal phosphorescence efficiency in an organic light-emitting device," *J. Appl. Phys.*, vol. 90, no. 10, pp. 5048–5051, 2001.
- [28] K.-J. Baeg, M. Binda, D. Natali, M. Caironi, and Y.-Y. Noh, "Organic light detectors: Photodiodes and phototransistors," *Adv. Mater.*, vol. 25, no. 31, pp. 4267–4295, Mar. 2013.
- [29] H. Aziz, Z. D. Popovic, N.-X. Hu, A.-M. Hor, and G. Xu, "Degradation mechanism of small molecule-based organic light-emitting devices," *Science*, vol. 283, no. 5409, pp. 1900–1902, 1999.
- [30] R. R. Schaller, "Moore's law: Past, present and future," *IEEE Spectr.*, vol. 34, no. 6, pp. 52–59, Jun. 1997.
- [31] J. B. Bates, N. J. Dudney, B. Neudecker, A. Ueda, and C. D. Evans, "Thin-film lithium and lithium-ion batteries," *Solid State Ionics*, vol. 135, no. 1, pp. 33–45, 2000.



Vishak Venkatraman received the Ph.D. degree in electrical engineering from the University of Cincinnati, Cincinnati, OH, USA, in 2017. His research, under the supervision of Prof. A. Steckl, was focused on the development of lab on chip biosensor devices with integrated organic optoelectronic devices. He is currently a Post-Doctoral Fellow with Northwestern University.



Andrew J. Steckl (S'70–M'73–SM'79–F'99–LF'13) received the B.S.E. degree in electrical engineering from Princeton University, Princeton, NJ, USA, in 1968, and the M.Sc. and Ph.D. degrees from the University of Rochester, Rochester, NY, USA, in 1970 and 1973, respectively.

From 1972 to 1976, he worked on infrared devices (at Honeywell) and charge coupled devices (at Rockwell). In 1976, he joined the Electrical, Computer and Systems Engineering Department, Rensselaer Polytechnic Institute, Troy, NY, USA, where he developed a research program in microfabrication of Si devices. In 1981, he founded the Center for Integrated Electronics, a multi-disciplinary academic center focused on VLSI research and teaching. In 1988, he joined the Electrical Engineering and Computer Science Department, University of Cincinnati, as an Ohio Eminent Scholar and a Gieringer Professor of Solid State Microelectronics. At the University of Cincinnati, he has built the Nanoelectronics Laboratory in the general area of semiconductor materials and devices. Current activities include organic light emitting and detecting diodes, microfluidic devices for point-of-use diagnostics, and electrospinning of complex fiber membranes for chemical and biomedical applications. His research has resulted in over 430 publications and 25 patents.

Dr. Steckl's awards and honors include the Rieveschl Award for Distinguished Scientific Research. He is a Fellow of the National Academy of Inventors and the American Association for the Advancement of Science.